Theoretical investigation of the electron transfer dynamics and photodegradation pathways in a hydrogen-evolving ruthenium-palladium photocatalyst

Magdalena Staniszewska[1], Stephan Kupfer*[2] and Julien Guthmuller*[1]

[1]Faculty of Applied Physics and Mathematics, Gdańsk University of Technology, Narutowicza 11/12, 80233 Gdańsk, Poland

[2]Institute of Physical Chemistry and Abbe Center of Photonics, Friedrich Schiller University Jena, Helmholtzweg 4, 07743 Jena, Germany

Abstract

Time-dependent density functional theory calculations combined with the Marcus theory of electron transfer (ET) were applied on the molecular photocatalyst $[(tbbpy)_2Ru(tpphz)PdCl_2]^{2+}$ in order to elucidate the light-induced relaxation pathways populated upon excitation in the longer wavelength range of its absorption spectrum. The computational results show that after the initial excitation, metal (Ru) to ligand (tpphz) charge transfer (MLCT) triplet states are energetically accessible, but that an ET toward the catalytic center ($PdCl_2$) from these states is a slow process, with estimated time constants above 1 ns. Instead, the calculations predict that low-lying Pd-centered states are efficiently populated - associated to an energy transfer toward the catalytic center. Thus, it is postulated that these states lead to the dissociation of a Cl^- and are consequently responsible for the experimentally observed degradation of the catalytic center. Following dissociation, it is shown that the ET rates from the MLCT states to the charge separated states are significantly increased (*i.e.* 10^5-10^6 times larger). This demonstrates that alteration of the catalytic center generates efficient charge separation.

1. Introduction

The development of devices and materials for the conversion of solar energy into electricity or into energy-rich chemicals (*i.e.* solar fuel) is a highly active field of research in chemistry and physics. For example, the commercial production of electricity from solar light is dominated by silicon solar cells, but many novel materials are under investigation in research laboratories[1],[2],[3],[4], *e.g.* dye-sensitized solar cells, quantum dot-sensitized solar cells, or organometal halide perovskite solar cells. Additionally, extensive efforts are conducted to develop photocatalytic systems for the production of solar fuels such as molecular hydrogen or small carbon-based molecules. In the context of the photocatalytic splitting of water into molecular hydrogen and oxygen, several hydrogen-evolving molecular photocatalysts were reported in the last decades[5],[6],[7],[8]. These systems consist typically of a photosensitizer, of a bridging ligand (*i.e.* electron relay) and of a catalytic center, where the molecular hydrogen in formed. The optimization of these so-called three-components system requires a precise understanding of the interplay between light absorption, electron transfer (ET) kinetics and catalytic turnover. To this aim, theoretical methods offer an opportunity to investigate the underlying molecular properties responsible for light absorption and to assess the subsequent excited state relaxation cascades, (*i.e.* ET processes) as well as to predict how these processes are affected by structural modifications of the photocatalyst or by its environment (*e.g.* solvent).

This contribution focuses on the supramolecular photocatalyst $[(tbbpy)_2Ru(tpphz)PdCl_2]^{2+}$ (Figure 1), which will be denoted **$RuPdCl_2$**. This system was introduced in 2006 by Sven Rau *et al.*[8] and has since then be the subject of many experimental and computational studies[9],[10],[11],[12],[13],[14],[15] to understand its photophysical properties and photocatalytic activity. Several related systems were subsequently synthesized in order to improve the stability of the photocatalyst and to optimize the catalytic turnover[14],[16],[17],[18],[19]. To realize light-driven hydrogen production, the catalytic site must undergo double photoreduction. In **$RuPdCl_2$** and in related systems, the commonly accepted mechanism for the first photo-induced ET from the

photosensitizer toward the catalytic center involves the following steps: (i) The photoexcitation in the first absorption band leads to the population of metal-to-ligand charge transfer (MLCT) states localized on the tpphz and tbbpy ligands, (ii) relaxation processes in the excited states leading to the population of triplet MLCT state(s) centered on the tpphz bridging ligand, and (iii) ET to the catalytic center leading to the reduction of the palladium and thus to the formation of a charge separated state. The latter step was assumed to occur in conjunction with the dissociation of a Cl^- [8],[9], and according to time-resolved measurements[9] this step has a characteristic time constant of 310 ps in acetonitrile. Due to the sub-nanosecond time scale of this process, re-reduction of the Ru center by the sacrificial electron donor (*e.g.* triethylamine) is supposed to occur only after the formation of the charge separated state. Furthermore, an intriguing property of the **$RuPdCl_2$** system is that its catalytic efficiency depends on the excitation wavelength[10]. This property has been correlated to the nature of the initially populated excited state, *i.e.* a higher catalytic efficiency is observed upon excitation in the longer wavelength region (around 500 nm) of the absorption band (populating tpphz MLCT states) than upon excitation at shorter wavelengths, where tbbpy MLCT states have a stronger contribution to the absorbance. Additionally, it has been shown that excitation at longer wavelengths results in the direct population of a singlet MLCT state centered on the phenazine part of the tpphz ligand[11],[13]. In the time scale of a few picoseconds[13], this state leads via intersystem crossing (ISC) to the population of triplet MLCT states with similar orbital characteristics. Recently, it has also be proven that during catalysis the **$RuPdCl_2$** system undergoes an alteration of the $PdCl_2$ catalytic center, that results in the formation of metal colloids[14], whereas similar compounds based on a platinum catalytic center are stable and present a different catalytic mechanism without the involvement of colloids[16]. The exact role of Pd colloids in the catalytic process of **$RuPdCl_2$** still needs to be determined.

The general motivation for theoretical studies of the ET kinetics in photocatalysts is to reveal the possible reaction pathways and predict their rates, as well as to understand how the initial excitation, the structural parameters or the environment influence the charge separation and the

charge recombination processes. To progress within this goal, the photo-induced ET of **$RuPdCl_2$** is investigated assuming an initial excitation in the longer wavelength part of the absorption spectrum. Despite theoretical investigations[11],[13] of the absorption spectrum, resonance Raman intensities and triplet excited state properties, the ET processes in **$RuPdCl_2$** were never investigated from a theoretical point of view. Moreover, in order to estimate the effect of Cl^- dissociation on the ET rates, the system $[(tbbpy)_2Ru(tpphz)PdCl]^{3+}$ (denoted **$RuPdCl_1$**) is investigated. The ET rates of both systems are determined using the semi-classical Marcus theory[20],[21], following a methodology recently employed to describe the ET processes in the related bimetallic complex[22] $[(bpy)_2Ru^{II}(tpphz)Co^{III}(bpy)_2]^{5+}$. In the Marcus picture, ET processes proceed between the diabatic potential energy curves (PECs) of the initial state (reactant) and of the final state (product) described as parabolas having identical frequencies ω, but displaced along a reaction coordinate. Rare thermal fluctuations of the surrounding environment lead to structural variations within the reactant that may lead in consequence to an ET between the two diabatic states in the vicinity of their crossing. The kinetics of the temperature-dependent ET dynamics are then governed by the reaction's driving force (ΔG), the reorganization energy (λ, the energy needed to distort the initial state into the structure of the final state and *vice versa*) and by the electronic coupling between both states at the crossing region.

The paper is organized as follows: Section 2 presents the quantum chemistry methods and the methodology used to estimate ET rates. Section 3.1 describes the singlet and triplet excited state properties at the ground state geometry. Sections 3.2 and 3.3 provide an investigation of the ET processes for **$RuPdCl_2$**. Section 3.4 reports the calculated excited states properties and ET rates of **$RuPdCl_1$**. Finally, discussions and conclusions are given in Section 4.

2. Theoretical methods

2.1 Quantum chemistry calculations

All quantum chemical calculations were performed with the Gaussian 09 program[23], which provided the structural and electronic properties of the **$RuPdCl_2$** and **$RuPdCl_1$** complexes. To reduce the computational cost of the calculations without affecting the properties, the structures of the complexes were simplified by replacing the *tert*-butyl groups by methyl groups (Figure 1). The equilibrium geometry of the singlet ground state (S_0) was obtained by means of density functional theory (DFT) using the B3LYP exchange-correlation (XC) functional[24],[25]. Harmonic vibrational frequencies were computed to confirm that the optimized structures correspond to minima on the potential energy surface. The 28-electron relativistic effective core potential MWB[26] was used with its basis set for the ruthenium and palladium atoms, while the 6-31G(d) basis set[27] was employed for the main group elements. Vertical excitation energies, oscillator strengths and electronic characters of the 100 lowest singlet and 100 lowest triplet excited states were calculated with time-dependent DFT (TDDFT). These calculations were performed at the S_0 geometry using the same XC functional, basis sets and core potentials. Additionally, the geometries of several excited states playing a role in the ET were optimized with TDDFT. Due to the ability of this computational setup to give a balanced description of ground and excited state properties for electronic states of different nature, *i.e.*, MLCT, intra-ligand charge transfer, intra-ligand, ligand-to-ligand charge transfer and metal-centered states, it was already successfully applied in order to elucidate the UV-vis absorption, resonance Raman, spectro-electrochemistry and ET dynamics in structurally closely related transition metal complexes[11],[12],[13],[22],[28],[29],[30]. The effects of the interaction with a solvent (acetonitrile, ε = 35.688, n = 1.344) were taken into account for the ground state and the excited states properties by the integral equation formalism of the polarizable continuum model[31] (IEFPCM). The nonequilibrium procedure of solvation was used for the calculation of the vertical singlet-singlet and singlet-triplet excitation energies at the different geometries, which is well-adapted for processes where only the fast reorganization of the electronic

distribution of the solvent is important. In contrast, the equilibrium procedure of solvation was applied for the excited state geometry optimizations.

2.2 Electron transfer kinetics

To access the non-adiabatic photo-induced ET processes in **RuPdCl$_2$** and **RuPdCl$_1$** the semi-classical Marcus theory is applied. In Marcus theory such ET dynamics proceed along the parabolic diabatic PECs of the electron donor state (D) and the acceptor state (A) along the reaction coordinate R_{ET}. Structural distortion within the donor state - induced by thermal fluctuations of the surrounding bath (*e.g.* solvent) - may provide sufficient electronic coupling between D and A to allow the ET to occur. The rate equation for such ET process is then given by:

$$k_{ET} = \frac{2\pi}{\hbar}\left|V_{D/A,\,max}\right|^2 (4\pi\lambda k_B T)^{-1/2} \exp\left(-\frac{(\Delta G+\lambda)^2}{4\lambda k_B T}\right), \quad (1)$$

here $V_{D/A,max}$ corresponds to the maximum potential coupling matrix element between the electron donor state D and the electron acceptor state A at the crossing point, λ to the reorganization energy, ΔG to the driving force of the ET (Gibbs free energy) and T (295 K) to the temperature. In case of **RuPdCl$_2$** and **RuPdCl$_1$** all investigated donor and acceptor states are of triplet multiplicity. The ET kinetics for the different pairs of D/A states was described along a linear-interpolated Cartesian coordinate (LICC) connecting the optimized equilibrium structures of the donor and acceptor states. The diabatic PECs for D and A were constructed along the LICC (denoted R_{ET}) by means of TDDFT single point calculations.

In order to calculate the potential coupling matrix elements between D and A along R_{ET}, a straightforward diabatization of the PECs was achieved by manually following the electronic transitions for each state of interest along the LICC. The adiabatic and diabatic PECs were then obtained by a cubic (B-)spline interpolation along R_{ET} using a total number of 100 grid points. The potential couplings V_{ij} are then retrieved by an unitary transformation of the adiabatic potential matrix V_i^{ad} for each R_{ET}:

$$\begin{pmatrix} V_1 & \cdots & V_{1n} \\ \vdots & \ddots & \vdots \\ V_{n1} & \cdots & V_n \end{pmatrix} = U^{\dagger} \begin{pmatrix} V_1^{\mathrm{ad}} & \cdots & 0 \\ \vdots & \ddots & \vdots \\ 0 & \cdots & V_n^{\mathrm{ad}} \end{pmatrix} U\,, \qquad (2)$$

where U is a general rotation matrix.

In a previous computational study on the photo-induced intra-molecular ET dynamics in $[(bpy)_2Ru^{II}(tpphz)Co^{III}(bpy)_2]^{5+}$ this computational protocol was evaluated against quantum dynamical wavepacket simulations, and both methods were found to be in very good agreement[22]. Besides of the application of quantum dynamics[22],[32],[33],[34],[35],[36] and path integral methods,[37],[38] the majority of computational studies addressing ET kinetics are focused on the comparison of semi-classical Marcus theory and molecular dynamical simulations.[39],[40],[41],[42],[43],[44],[45],[46]

3. Results

3.1 Excited states involved in the initial photoactivation

The absorption spectrum of **RuPdCl$_2$** ([(tbbpy)$_2$Ru(tpphz)PdCl$_2$]$^{2+}$) simulated in acetonitrile with a PCM is given in Figure 1. The absorption in the visible range is dominated by a MLCT band, which - according to the calculations - consists mainly of a superposition of six singlet excitations of non-negligible oscillator strengths (Table 1). As described in previous works[11],[13], the low-energy states (S_2 and S_{13}) involve MLCT transitions to the tpphz bridging ligand (BL), the high-energy state S_{19} presents transitions to the bpy ligands, while the excited states S_{15}, S_{16} and S_{17} show an overlap of MLCT transitions to both tpphz and bpy ligands. The calculated absorption maximum is obtained at 2.96 eV, which is in reasonable agreement with the experimental value of 2.79 eV (*i.e.* 445 nm) measured in acetonitrile[8]. This is a typical accuracy for TDDFT calculations on ruthenium complexes (see *e.g.* references[47],[48],[49]), showing that the B3LYP XC functional provides an adequate reproduction of the excited state energies, whereas XC functionals with larger percentage of exact exchange were proven to be less accurate for **RuPdCl$_2$**[11].

The main goal of this work is to unravel the possible excited state relaxation channels populated upon excitation in the longer wavelength range of the absorption spectrum (*i.e.* around 500 nm). The analysis of the singlet excited states reveals that an excitation in this wavelength region will lead predominantly to the population of the S_2 state (Figure 1). This state corresponds to a direct MLCT to the bridging ligand (Table 1), which populates the LUMO, π^*_{BL1}, centered on the phenazine part of the tpphz ligand (Figure 2). It is well-known for ruthenium complexes that upon singlet excitation ultrafast population transfer to the triplet manifold occurs by ISC, followed by energy dissipation along the excited states relaxation pathways. Therefore, by assuming an excitation in the S_2 state, the energetic position of the nearby triplet states is firstly investigated at the S_0 geometry (Table 1).

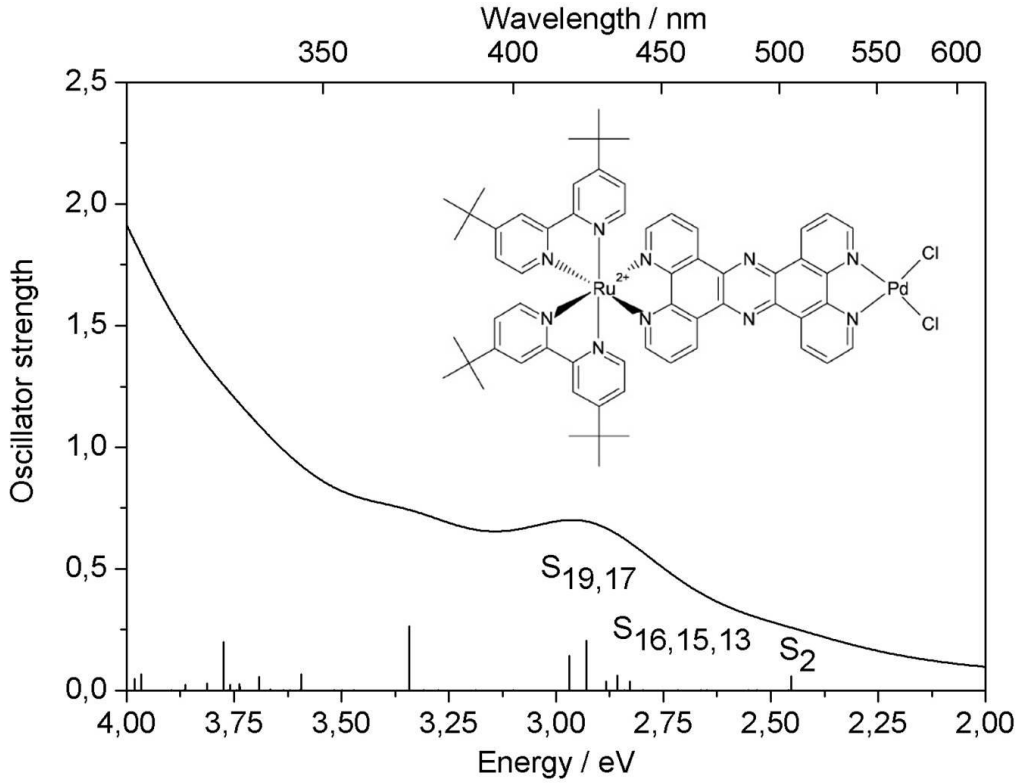

Figure 1. Calculated absorption spectrum of **$RuPdCl_2$**. A Lorentzian function with a FWHM of 4000 cm^{-1} is employed to broaden the transitions. The six main singlet MLCT states are indicated.

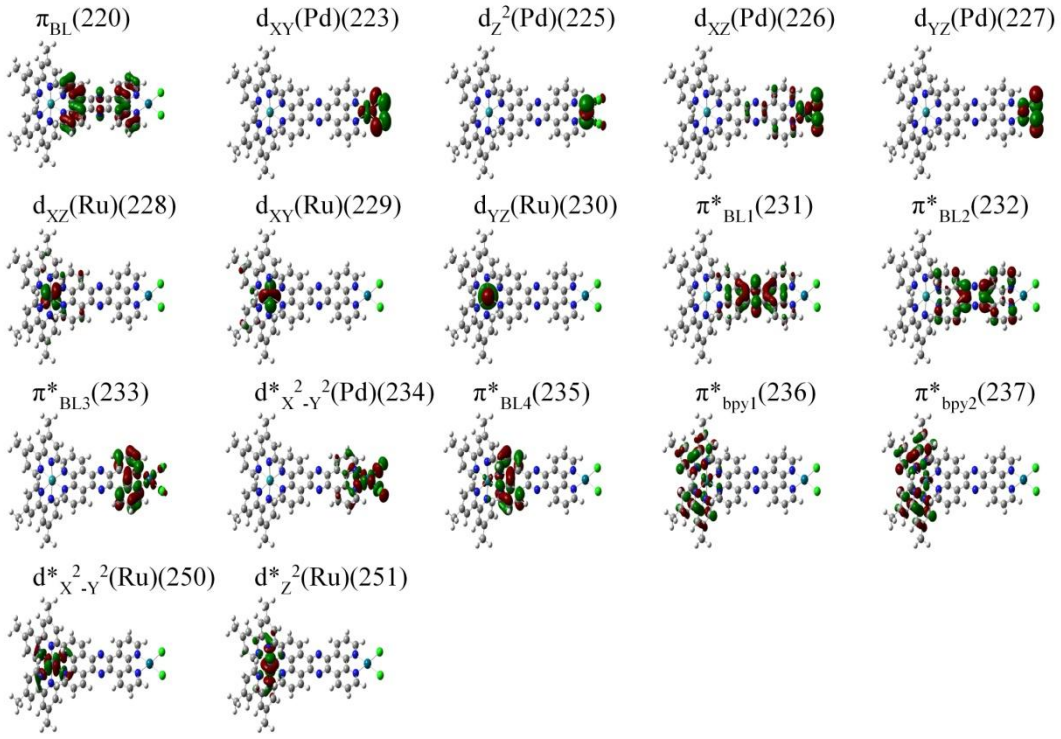

Figure 2. Frontier orbitals of **$RuPdCl_2$** and employed nomenclature including the orbital numbering at the S_0 geometry.

Table 1. Vertical excitation energies (VEE), wavelengths (λ), oscillator strengths (f) and singly-excited configurations of the main singlet and triplet excited states calculated at the S_0 geometry for **$RuPdCl_2$**.

State	Transition	Weight (%)[a]	VEE (eV)	λ (nm)	f
singlet-singlet excitations					
S_2	$d_{XZ}(Ru) \rightarrow \pi^*_{BL1}$	96	2.45	506	0.058
S_{13}	$d_{XY}(Ru) \rightarrow \pi^*_{BL2}$ $d_{XZ}(Ru) \rightarrow \pi^*_{BL4}$	67 26	2.83	438	0.036
S_{15}	$d_{XZ}(Ru) \rightarrow \pi^*_{bpy1}$ $d_{XZ}(Ru) \rightarrow \pi^*_{BL4}$ $d_{XY}(Ru) \rightarrow \pi^*_{BL2}$	41 36 16	2.86	434	0.062
S_{16}	$d_{XZ}(Ru) \rightarrow \pi^*_{BL2}$ $d_{XY}(Ru) \rightarrow \pi^*_{bpy1}$ $d_{XZ}(Ru) \rightarrow \pi^*_{bpy2}$	62 20 12	2.88	430	0.037
S_{17}	$d_{XY}(Ru) \rightarrow \pi^*_{bpy2}$ $d_{XZ}(Ru) \rightarrow \pi^*_{bpy1}$ $d_{XZ}(Ru) \rightarrow \pi^*_{BL4}$ $d_{XY}(Ru) \rightarrow \pi^*_{BL2}$	40 23 21 11	2.93	423	0.205
S_{19}	$d_{XZ}(Ru) \rightarrow \pi^*_{bpy2}$ $d_{XY}(Ru) \rightarrow \pi^*_{bpy1}$	52 44	2.97	418	0.142
singlet-triplet excitations					
T_1 ($T_{Pd\_Z^2}$)	$d_{Z^2}(Pd) \rightarrow d^*_{X^2-Y^2}(Pd)$ $d_{Z^2}(Pd) \rightarrow \pi^*_{BL3}$	80 18	1.71	724	0.000
T_2 (T_{Pd_YZ})	$d_{YZ}(Pd) \rightarrow d^*_{X^2-Y^2}(Pd)$ $d_{YZ}(Pd) \rightarrow \pi^*_{BL3}$	70 16	1.87	662	0.000
T_3 (T_{Pd_XZ})	$d_{XZ}(Pd) \rightarrow d^*_{X^2-Y^2}(Pd)$ $d_{XZ}(Pd) \rightarrow \pi^*_{BL3}$	61 14	2.02	614	0.000
T_4 (T_{BL1_YZ})	$d_{YZ}(Ru) \rightarrow \pi^*_{BL1}$ $d_{YZ}(Ru) \rightarrow \pi^*_{BL4}$	59 27	2.23	554	0.000
T_5 (T_{Pd_XY})	$d_{XY}(Pd) \rightarrow d^*_{X^2-Y^2}(Pd)$ $d_{XY}(Pd) \rightarrow \pi^*_{BL3}$	70 16	2.34	529	0.000
T_6 (T_{BL1_XZ})	$d_{XZ}(Ru) \rightarrow \pi^*_{BL1}$ $d_{XZ}(Ru) \rightarrow \pi^*_{BL4}$ $d_{XZ}(Ru) \rightarrow \pi^*_{bpy1}$	54 31 10	2.36	524	0.000
T_7 (T_{BL4_YZ})	$d_{YZ}(Ru) \rightarrow \pi^*_{BL1}$ $d_{YZ}(Ru) \rightarrow \pi^*_{BL4}$ $d_{YZ}(Ru) \rightarrow \pi^*_{bpy1}$	36 24 10	2.38	521	0.000
T_8 (T_{BL4_XZ})	$d_{XZ}(Ru) \rightarrow \pi^*_{BL1}$ $d_{XZ}(Ru) \rightarrow \pi^*_{BL4}$ $d_{XZ}(Ru) \rightarrow \pi^*_{bpy1}$	37 24 13	2.44	508	0.000
T_9 (T_{BL1_XY})	$d_{XY}(Ru) \rightarrow \pi^*_{BL1}$	76	2.44	507	0.000
T_{14} (T_{BL2_YZ})	$d_{YZ}(Ru) \rightarrow \pi^*_{BL2}$	79	2.65	468	0.000
T_{16} (T_{BL4_XY})	$d_{XY}(Ru) \rightarrow \pi^*_{BL4}$	61	2.69	461	0.000
T_{19} (T_{BL2_XZ})	$d_{XZ}(Ru) \rightarrow \pi^*_{BL2}$ $\pi_{BL}(220) \rightarrow \pi^*_{BL1}$ $d_{XZ}(Ru) \rightarrow \pi^*_{bpy2}$	36 17 14	2.83	438	0.000
T_{20} (T_{BL2_XY})	$d_{XY}(Ru) \rightarrow \pi^*_{BL2}$	82	2.83	437	0.000
T_{21} (T_{BL3_YZ})	$d_{YZ}(Ru) \rightarrow \pi^*_{BL3}$ $d_{YZ}(Ru) \rightarrow d^*_{X^2-Y^2}(Pd)$	84 14	2.95	420	0.000
T_{24} (T_{CS_YZ})	$d_{YZ}(Ru) \rightarrow d^*_{X^2-Y^2}(Pd)$ $d_{YZ}(Ru) \rightarrow \pi^*_{BL3}$	85 14	3.02	410	0.000
T_{25} (T_{BL3_XZ})	$d_{XZ}(Ru) \rightarrow \pi^*_{BL3}$ $d_{XZ}(Ru) \rightarrow d^*_{X^2-Y^2}(Pd)$	71 13	3.08	402	0.000
T_{27} (T_{BL3_XY})	$d_{XY}(Ru) \rightarrow \pi^*_{BL3}$ $d_{XY}(Ru) \rightarrow d^*_{X^2-Y^2}(Pd)$	82 13	3.11	398	0.000
T_{29} (T_{CS_XZ})	$d_{XZ}(Ru) \rightarrow d^*_{X^2-Y^2}(Pd)$ $d_{XZ}(Ru) \rightarrow \pi^*_{BL3}$	82 16	3.17	391	0.000
T_{30} (T_{CS_XY})	$d_{XY}(Ru) \rightarrow d^*_{X^2-Y^2}(Pd)$ $d_{XY}(Ru) \rightarrow \pi^*_{BL3}$	85 14	3.17	390	0.000

[a] Weights larger than 10%.

Table 1 shows that the nine lowest triplet states have an energy below the S_2 state energy (2.45 eV) and are, therefore, energetically directly accessible from S_2. These states correspond to (i) the three T_{BL1} states (T_4, T_6 and T_9), which consist mainly of MLCT transitions from the d_{YZ}(Ru), d_{XZ}(Ru) and d_{XY}(Ru) orbitals to the π^*_{BL1} orbital (Figure 2), respectively, (ii) the two triplet states T_7 and T_8, which involve a strong mixing of MLCT transitions to the π^*_{BL4} and π^*_{BL1} orbitals and are referred here as the T_{BL4_YZ} and T_{BL4_XZ} states, respectively, and (iii) the four Pd-centered states (T_1, T_2, T_3 and T_5), which correspond to transitions from the occupied Pd orbitals d_Z^2(Pd), d_{YZ}(Pd), d_{XZ}(Pd) and d_{XY}(Pd) to the unoccupied orbital $d^*_{X^2-Y^2}$(Pd), respectively. Furthermore, Table 1 presents all higher energy states (up to state T_{30}) that involve an ET from the ruthenium toward the bridging ligand or the catalytic center. This concerns (i) the third T_{BL4} state (T_{16}), (ii) the three T_{BL2} (T_{14}, T_{19} and T_{20}) and the three T_{BL3} (T_{21}, T_{25} and T_{27}) states, and (iii) the three charge separated (CS) states T_{CS} (T_{24}, T_{29} and T_{30}), which correspond to transitions from a Ru orbital to the Pd orbital $d^*_{X^2-Y^2}$(Pd). The complete list of the 30 lowest triplet excited states is given in the Table S1 and Figure S1. The remaining states consist of MLCT excitations to the terminal bpy ligands, of tpphz centered excitations, of MLCT excitations from the Pd atom to the tpphz ligand as well as a Ru-centered state.

Geometry optimizations for the S_2 state and for the nine lowest triplet excited states were performed at the TDDFT level of theory in order to investigate ET processes based on the semi-classical Marcus theory. Minima of the potential energy surfaces were obtained for the S_2 state, for the three T_{BL1} states and for the four T_{Pd} states, whereas the geometry optimizations of the two T_{BL4} states (T_7 and T_8) converged to the minima of the T_{BL1_YZ} and T_{BL1_XZ} states, respectively. The strong mixing between the T_{BL1} and T_{BL4} states is probably responsible of the state crossing occurring during the optimization and of the inability of the algorithm to find minima for these two T_{BL4} states. Additionally, the geometries of the three T_{CS} states were successfully optimized. These states are included to investigate possible ET toward the catalytic center. The geometries of the other triplet states reported in Table 1 were not considered in this study, as it may be assumed that

they are predominantly populated via excitations to higher singlet excited states. Similarly, the contributions of triplet MLCT states to the bpy sphere and of states describing charge recombination processes are not investigated here.

3.2 Electron transfer associated to charge separation in **$RuPdCl_2$**

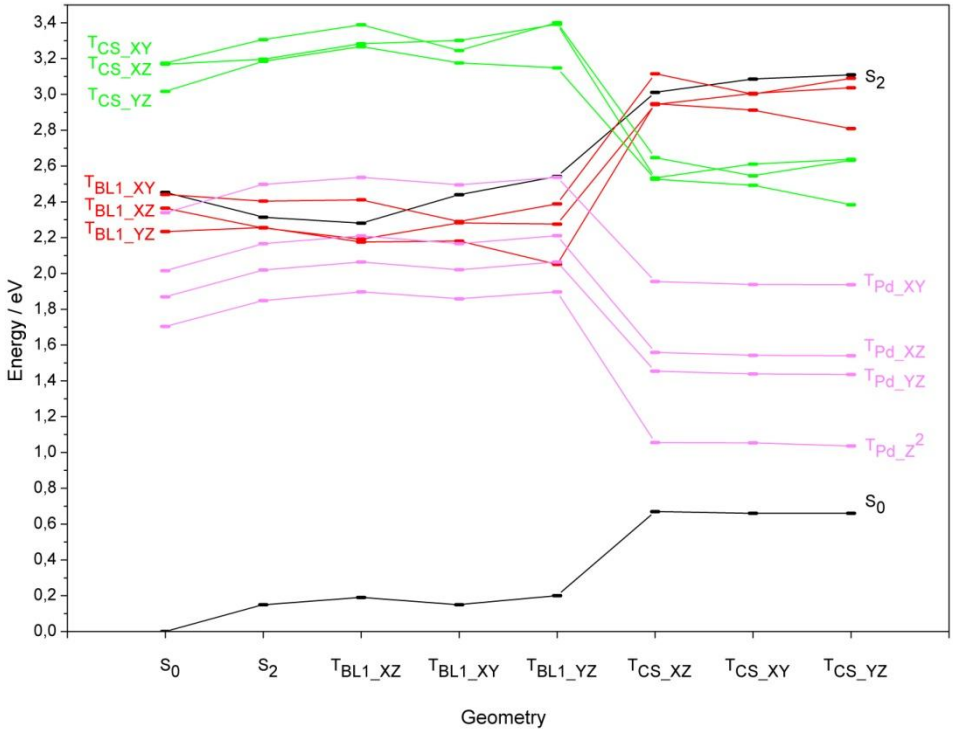

Figure 3. Relative energies of the states of interest at different optimized geometries. Black: the singlet states S_0 and S_2, Red: the three T_{BL1} states, Green: the three T_{CS} states, Pink: the four T_{Pd} states.

Upon excitation to S_2, ultrafast population transfer occurs to the triplet states via ISC. It can be assumed that this population transfer occurs most likely to the T_{BL1} states because they have similar energies and orbital characters as the S_2 state (Table 1). Furthermore, the energetic proximity of the T_{BL1} states with the S_2 state is maintained upon equilibration of S_2. Indeed, the energies of the S_2 and T_{BL1} states follow a comparable evolution when going from the S_0 state geometry to the S_2 and T_{BL1} states geometries (Figure 3), which is understood from the fact that these states differ merely in the position of the electron hole at the ruthenium and feature a spinflip in π^*_{BL1}. After population of the T_{BL1} states - representing a hole at the ruthenium and an electron

localized on the bridging ligand - the question arises, whether a direct ET to the catalytic center is possible from the T_{BL1} states. As revealed in Figure 3 the three CS states, T_{CS}, undergo considerable stabilization (by about 0.5-1.0 eV) from the Franck-Condon region toward their respective equilibrium geometries, accompanied by a similar destabilization of the T_{BL1} states, which leads to a crossing of the respective diabatic PECs.

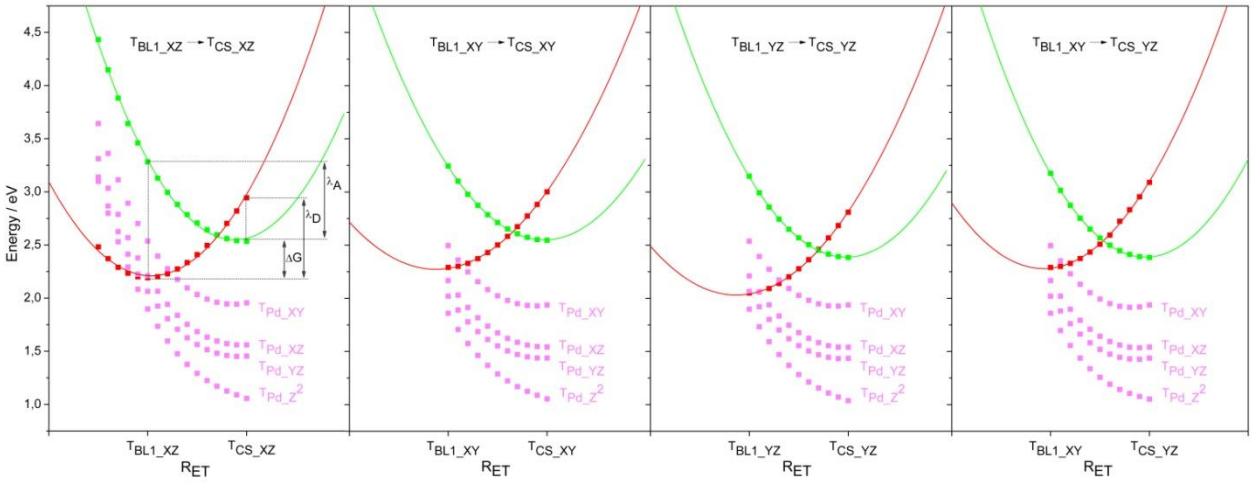

Figure 4. Calculated diabatic PECs of four pairs of donor (T_{BL1}, red squares) and acceptor (T_{CS}, green squares) states obtained at the TDDFT level of theory along a LICC (R_{ET}). A quadratic polynomial was fitted to the data sets. The energies of the four T_{Pd} states (pink squares) are indicated.

The ET rates between the T_{BL1} and T_{CS} states are investigated using semi-classical Marcus theory as introduced in section 2.2. The three pairs of donor and acceptor states $T_{BL1\_XZ} \rightarrow T_{CS\_XZ}$, $T_{BL1\_XY} \rightarrow T_{CS\_XY}$ and $T_{BL1\_YZ} \rightarrow T_{CS\_YZ}$ are considered, in which it is assumed that the singly occupied ruthenium orbital remains unchanged and ET proceeds from π^*_{BL1} toward $d^*_{X^2-Y^2}(Pd)$. Moreover, the pair $T_{BL1\_XY} \rightarrow T_{CS\_YZ}$ is also considered because it involves the donor state (T_{BL1_XY}) and the acceptor state (T_{CS_YZ}) with the highest and lowest energies, respectively. For each pair of states, additional TDDFT calculations were performed along a LICC (denoted R_{ET}) in order to construct the diabatic PECs of the donor and acceptor states (Figure 4). The obtained PECs have a typical parabolic shape and were therefore fitted by a quadratic polynomial. This shows that the one-dimensional LICC is an appropriate coordinate to describe the ET process between the T_{BL1}

and T_{CS} states within the Marcus theory. However, the curvature of the donor and acceptor PECs are not exactly identical, which leads to two values of the reorganization energy (*i.e.* λ_D and λ_A, see Figure 4 and Table 2). Furthermore, the potential coupling ($V_{D/A}$) was calculated from an unitary transformation performed at each grid point along the ET coordinate (Equation 2). Table 2 shows that the $T_{BL1\_XZ} \rightarrow T_{CS\_XZ}$ and $T_{BL1\_YZ} \rightarrow T_{CS\_YZ}$ pairs have comparable driving forces, reorganization energies and maximum potential couplings ($V_{D/A,max}$ obtained at the crossing region), whereas the $T_{BL1\_XY} \rightarrow T_{CS\_XY}$ and $T_{BL1\_XY} \rightarrow T_{CS\_YZ}$ pairs feature smaller driving forces and potential couplings.

Table 2. Driving forces (ΔG), reorganization energies (λ_D and λ_A), potential couplings ($V_{D/A,max}$) and rate constants (k) for pairs of states.

donor → acceptor	ΔG (eV)	λ_i (eV)	$V_{D/A,max}$ (eV)	k_i (s^{-1})	$1/k_i$ (ns)
$T_{BL1\_XZ} \rightarrow T_{CS\_XZ}$	0.342	0.752 0.750	0.049	7.49×10^6 7.68×10^6	134 130
$T_{BL1\_XY} \rightarrow T_{CS\_XY}$	0.255	0.712 0.700	0.026	3.28×10^7 3.66×10^7	30.5 27.3
$T_{BL1\_YZ} \rightarrow T_{CS\_YZ}$	0.334	0.759 0.765	0.052	1.00×10^7 9.55×10^6	100 105
$T_{BL1\_XY} \rightarrow T_{CS\_YZ}$	0.094	0.800 0.792	0.025	6.59×10^8 7.12×10^8	1.52 1.40

The rate constant and its inverse were calculated for the four pairs of donor and acceptor states by means of semi-classical Marcus theory (Equation 1). The obtained rates lie between 7.49×10^6 and 7.12×10^8 s^{-1} (Table 2). In particular, the larger rates are found for the pairs starting from the T_{BL1_XY} donor states. This is mainly explained by the smaller driving forces that compensate for the lower potential couplings. Moreover, the smaller driving forces for these pairs of donor and acceptor states can be related to the higher energy of the T_{BL1_XY} state (Table 1 and Figure 4) in comparison to the other T_{BL1} states. In the case of the $T_{BL1\_XZ} \rightarrow T_{CS\_XZ}$ pair, additional points were computed along R_{ET} on the left side of the T_{BL1_XZ} minimum (Figure 4). The inclusion of these points into the fitted PECs provided slightly increased rates with values of 8.06×10^6 and 8.27×10^6 s^{-1}, whereas rates of 7.49×10^6 and 7.68×10^6 s^{-1}, respectively, were obtained considering points only in-between the donor and acceptor minima. Generally, the calculated rates for the pairs

of the T_{BL1} and T_{CS} states are small. This is attributed to the positive values of the driving force, which makes the ET energetically unfavorable. For example, using the same methodology to investigate the ET process between comparable T_{BL} and T_{CS} states of a related $[(bpy)_2Ru^{II}(tpphz)Co^{III}(bpy)_2]^{5+}$ complex[22] yielded negative driving forces and rates about 10^4-10^6 larger. Therefore, with inverse rate constants comprised between 1.40 ns and 134 ns, it is concluded that the direct ET from the T_{BL1} states to the T_{CS} states is a slow process for **$RuPdCl_2$**. Still, a faster indirect ET (*i.e.* $T_{BL1} \rightarrow T_{BL2,3,4} \rightarrow T_{CS}$) cannot entirely be excluded, but seems unlikely according to the higher energetic positions of the other T_{BL} states. Therefore, such a possibility is not investigated in the present study. However, as indicated by Figures 3 and 4, a transfer of population from the T_{BL1} states to the T_{Pd} states is energetically favorable.

3.3 Deactivation processes associated to Pd-centered states in **$RuPdCl_2$**

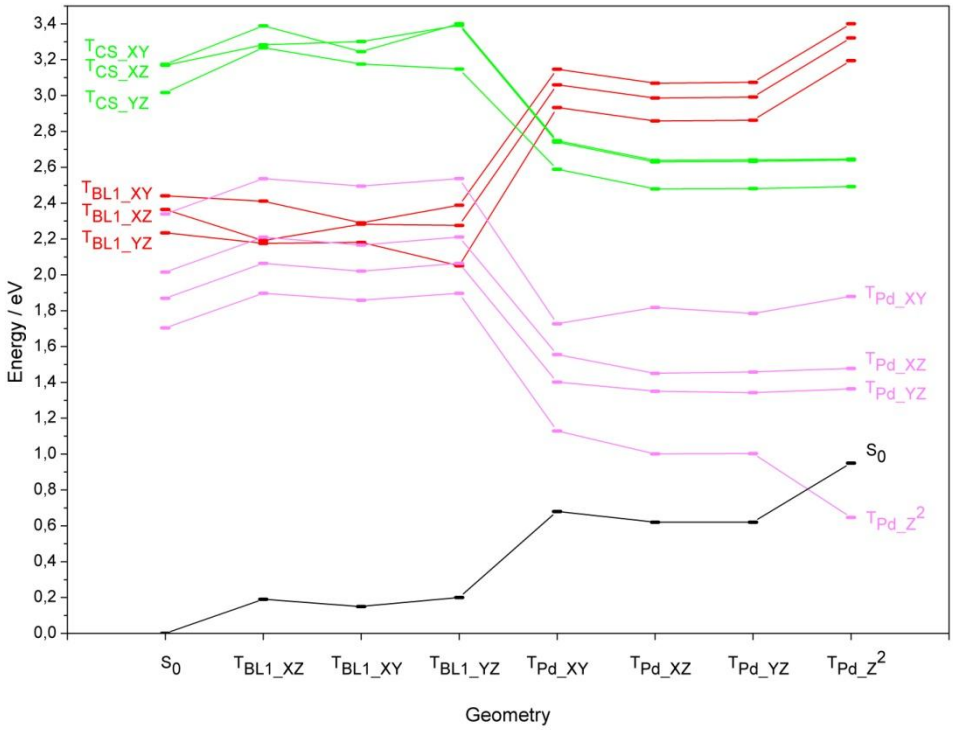

Figure 5. Relative energies of the states of interest at different optimized geometries. Black: the singlet state S_0, Red: the three T_{BL1} states, Green: the three T_{CS} states, Pink: the four T_{Pd} states.

The calculations predict in the Franck-Condon region four Pd-centered excited states with energies below or near the T_{BL1} states. The energetic position of these local excitations with respect to the MLCT states is corroborated by additional calculations (Tables S2 and S3), which were performed with the long-range corrected XC functional CAM-B3LYP[50] as well as by using the Tamm-Dancoff approximation of TDDFT together with the XC functional B3LYP (see *e.g.* reference[51]). The presence of T_{Pd} states in the low-energy region of **$RuPdCl_2$** has never been reported. As indicated by experimental studies of structurally related ruthenium-cobalt photocatalysts and of their precursors[52], such states can lead to deactivation processes. Therefore, the possible impact of T_{Pd} states on the photochemistry and on the excited state relaxation dynamics is investigated for the first time in **$RuPdCl_2$**. As it is seen from Figure 5, the energies of the Pd-centered states are stabilized by approximately 1 eV when going from the T_{BL1} to the T_{Pd}

geometries, whereas the T_{BL1} energies are increased by about the same amount. Hence, the relative energies of the states suggest a favorable population transfer between the T_{BL1} and the T_{Pd} states.

The ET rates between all twelve pairs of donor (three T_{BL1}) and acceptor (four T_{Pd}) states are investigated using Marcus theory. The population transfer between a T_{BL1} state and a T_{Pd} state describes a combined electron recombination from the tpphz ligand to the ruthenium, together with an energy transfer to the palladium, in which a palladium electron is excited from an occupied d(Pd) orbital to the anti-bonding orbital $d^*_{X^2-Y^2}$(Pd). The calculated diabatic PECs associated with the T_{BL1_XZ} state are given in Figure 6, while the other PECs are reported in Figures S3 and S4. The PECs were constructed by considering points between the donor and acceptor minima. Additional points were also included on the left side of the T_{BL1} state minimum in order to describe the so-called inverted Marcus region[53]. The PECs involving T_{Pd_XY}, T_{Pd_XZ} and T_{Pd_YZ} hold the typical parabolic shape, whereas the PEC of the $T_{Pd\_Z^2}$ state is non-harmonic and presents a discontinuity close to its minimum. It is also observed that at the $T_{Pd\_Z^2}$ geometry, the energy of the S_0 state is calculated higher than the energy of the $T_{Pd\_Z^2}$ state (Figure 5). This behavior can be related to the difficulty of DFT to properly describe the ground state wave function and energy at a significantly distorted geometry. Indeed, the $T_{Pd\_Z^2}$ state geometry presents the larger elongations of the Pd-Cl and Pd-N bond lengths with respect to the S_0 geometry, with variations of 0.19 and 0.28 Å, respectively (Table S4). Therefore, due to the non-parabolic shape of the $T_{Pd\_Z^2}$ PECs, the ET rates could not be determined for transfers to this state.

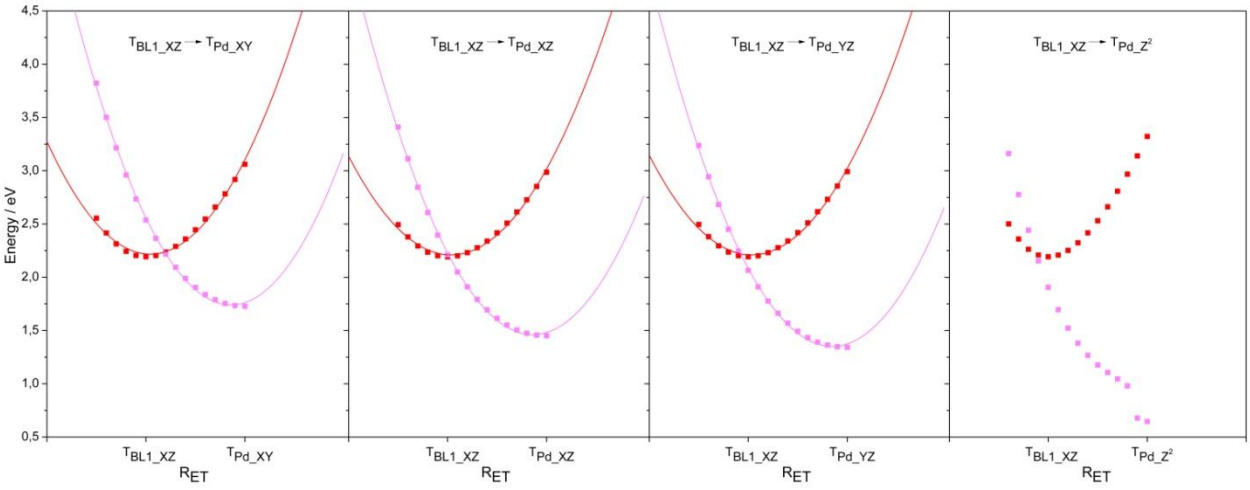

Figure 6. Calculated diabatic PECs of the four pairs of donor (T_{BL1_XZ}, red squares) and acceptor (T_{Pd}, pink squares) states obtained at the TDDFT level of theory along a LICC (R_{ET}). A quadratic polynomial was fitted to the data sets.

Table 3. Driving forces (ΔG), reorganization energies (λ_D and λ_A), potential couplings ($V_{D/A,max}$) and rate constants (k) for pairs of states.

donor → acceptor	ΔG (eV)	λ_i (eV)	$V_{D/A,max}$ (eV)	k_i (s^{-1})	$1/k_i$ (fs)
$T_{BL1\_XZ} \rightarrow T_{Pd\_XY}$	-0.464	0.869 0.809	0.063	1.11×10^{13} 1.73×10^{13}	90.1 57.8
$T_{BL1\_XZ} \rightarrow T_{Pd\_XZ}$	-0.741	0.794 0.760	0.063	7.35×10^{13} 7.75×10^{13}	13.6 12.9
$T_{BL1\_XZ} \rightarrow T_{Pd\_YZ}$	-0.849	0.800 0.723	0.066	7.95×10^{13} 6.93×10^{13}	12.6 14.4
$T_{BL1\_XY} \rightarrow T_{Pd\_XY}$	-0.563	0.857 0.768	0.062	2.59×10^{13} 4.30×10^{13}	38.6 23.3
$T_{BL1\_XY} \rightarrow T_{Pd\_XZ}$	-0.839	0.779 0.716	0.022	9.03×10^{12} 7.99×10^{12}	111 125
$T_{BL1\_XY} \rightarrow T_{Pd\_YZ}$	-0.949	0.784 0.678	0.027	9.95×10^{12} 5.21×10^{12}	101 192
$T_{BL1\_YZ} \rightarrow T_{Pd\_XY}$	-0.323	0.882 0.810	0.028	4.37×10^{11} 8.36×10^{11}	2290 1200
$T_{BL1\_YZ} \rightarrow T_{Pd\_XZ}$	-0.600	0.808 0.761	0.061	4.08×10^{13} 5.10×10^{13}	24.5 19.6
$T_{BL1\_YZ} \rightarrow T_{Pd\_YZ}$	-0.709	0.812 0.723	0.062	6.41×10^{13} 7.71×10^{13}	15.6 13.0

The calculated rates for the nine considered pairs of donor and acceptor states are comprised between 4.37×10^{11} and 7.95×10^{13} s^{-1} (Table 3). All driving forces indicate highly exergonic reactions and in most cases the ET processes are within the normal regime[54] of ET ($-\lambda < \Delta G < 0$). The exceptions concern the pairs $T_{BL1\_XZ} \rightarrow T_{Pd\_YZ}$, $T_{BL1\_XY} \rightarrow T_{Pd\_XZ}$ and $T_{BL1\_XY} \rightarrow T_{Pd\_YZ}$, in which the crossing occurs in the inverted region (*i.e.* $\Delta G < -\lambda$). It can also be mentioned that some

pairs have small activation energies or undergo barrier free ET (*i.e.* $\Delta G \approx -\lambda$), *e.g.* $T_{BL1\_XZ} \rightarrow T_{Pd\_XZ}$ (Table 3 and Figure 6). The smaller rate is obtained for the pair $T_{BL1\_YZ} \rightarrow T_{Pd\_XY}$, which features a small potential coupling of merely 0.028 eV and involves the energetically lowest donor state and highest acceptor state leading in consequence to the smallest absolute value of the driving force $|\Delta G| = 0.323$ eV. The largest absolute value of the driving force ($|\Delta G| = 0.949$ eV) is predicted for $T_{BL1\_XY} \rightarrow T_{Pd\_YZ}$ that involves the energetically highest donor state and lowest acceptor state. However, due to its small potential coupling (0.027 eV), this pair presents smaller rates than the pair $T_{BL1\_XZ} \rightarrow T_{Pd\_YZ}$, which has a larger potential coupling (0.066 eV) and a driving force close to $-\lambda$. Generally, the calculated rates for the $T_{BL1} \rightarrow T_{Pd}$ transfer are about 10^4-10^7 times larger than the rates obtained for the CS processes ($T_{BL1} \rightarrow T_{CS}$). These results clearly show that the population transfer from T_{BL1} to T_{Pd} states is very efficient and occurs with inverse rate constants comprised between 10 fs and 1 ps (Table 3). Therefore, due to the large difference in the time scale of ET to the T_{CS} and T_{Pd} states, it is concluded that, following population of the T_{BL1} states, ET will almost exclusively occur to the T_{Pd} states.

The T_{Pd} states as well as the T_{CS} states feature a reduced bond order of the Pd-N and Pd-Cl bonds due to the singly occupied $d^*_{X^2-Y^2}$(Pd) orbital, which will therefore weaken the Pd-Cl bonds. Indeed, the investigation of the T_{Pd} equilibrium geometries (Table S4) demonstrates that the Pd-Cl bonds undergo significant elongations of 0.05, 0.12, 0.11 and 0.19 Å from the S_0 geometry to the T_{Pd_XY}, T_{Pd_XZ}, T_{Pd_YZ} and $T_{Pd\_Z^2}$ geometries, respectively. Similarly, an elongation of 0.19 Å of the Pd-Cl bonds is obtained going from the S_0 geometry to the T_{CS} geometries. These results are in agreement with the proposed photo-induced mechanism[8],[9],[14] of **$RuPdCl_2$**, in which a dissociation of a chlorine ion was postulated. Therefore, it is reasonable to conjecture that the population of both the T_{Pd} and the T_{CS} states causes a Pd-Cl bond breaking, which leads in consequence to the release of Cl^-. Subsequent to the Pd-Cl cleavage, the system is assumed to relax to the electronic ground state of the newly formed compound (*i.e.* **$RuPdCl_1$**).

3.4 Electron transfer associated to charge separation in **$RuPdCl_1$**

The system **$RuPdCl_1$** ($[(tbbpy)_2Ru(tpphz)PdCl]^{3+}$) is considered in order to investigate the possible consequences of Cl^- release on the light-driven ET processes. Similarly to **$RuPdCl_2$**, the singlet and triplet excited state properties are first calculated at the S_0 geometry (Table 4). The absorption spectrum of **$RuPdCl_1$** (Figure S5) presents strong similarities with the spectrum of **$RuPdCl_2$** (Figure 1). The absorption in the visible range is dominated by a MLCT band, which consists of a superposition of MLCT transitions to the bpy ligands (S_{26} and S_{25} states) at lower wavelengths and to the tpphz bridging ligand (S_{21} and S_9 states) at longer wavelengths (Table 4). In particular, the S_9 state (2.35 eV) features an identical orbital character as the S_2 state (2.45 eV) of **$RuPdCl_2$** and corresponds to a MLCT transition to the π^*_{BL1} orbital. Therefore, an excitation in the longer wavelength range of the absorption spectrum (*i.e.* around 500 nm) of **$RuPdCl_1$** will lead predominantly to the population of the S_9 state.

Table 4 lists the eleven triplet states with energies below the S_9 state energy at the S_0 geometry. Similarly to **$RuPdCl_2$**, these states correspond to the three T_{BL1} states (T_8, T_9 and T_{11}), the four T_{Pd} states (T_1, T_2, T_3 and T_5) as well as one T_{BL4} state (T_{10}). Subsequently to the excitation into the S_9 state, ISC is assumed to occur most likely to the T_{BL1} states, which have similar energies and orbital characters as the S_9 state (Figure S7). However, contrary to **$RuPdCl_2$** the three T_{CS} states (T_4, T_6 and T_7) of **$RuPdCl_1$** are found below the S_9 and T_{BL1} states. This is due to a strong stabilization of the T_{CS} states by about 1.3 eV going from **$RuPdCl_2$** to **$RuPdCl_1$**. Therefore, the lower energetic position of the T_{CS} states is expected to favor the ET between the T_{BL1} and T_{CS} states. To investigate such a process, the geometries of the two lowest T_{BL1} states (T_{BL1_YZ} and T_{BL1_XZ}) and of the associated T_{CS} states (T_{CS_YZ} and T_{CS_XZ}) were successfully optimized, whereas the optimization of the higher T_{BL1_XY} state did not converge. The geometries of the other states (*e.g.* T_{Pd} or T_{BL4}) were not considered for **$RuPdCl_1$**.

Table 4. Vertical excitation energies (VEE), wavelengths (λ), oscillator strengths (f) and singly-excited configurations of the main singlet and triplet excited states calculated at the S_0 geometry for **$RuPdCl_1$**.

State	Transition	Weight (%)[a]	VEE (eV)	λ (nm)	f
singlet-singlet excitations					
S_9	$d_{XZ}(Ru) \rightarrow \pi^*_{BL1}$	94	2.35	527	0.043
S_{21}	$d_{XZ}(Ru) \rightarrow \pi^*_{BL4}$ $d_{XZ}(Ru) \rightarrow \pi^*_{bpy1}$	66 25	2.85	434	0.154
S_{25}	$d_{XZ}(Ru) \rightarrow \pi^*_{bpy1}$ $d_{XY}(Ru) \rightarrow \pi^*_{bpy2}$ $d_{XZ}(Ru) \rightarrow \pi^*_{BL4}$	41 39 12	2.92	424	0.127
S_{26}	$d_{XZ}(Ru) \rightarrow \pi^*_{bpy2}$ $d_{XY}(Ru) \rightarrow \pi^*_{bpy1}$	50 46	2.98	415	0.149
singlet-triplet excitations					
T_1 ($T_{Pd\_Z^2}$)	$d_{Z^2}(Pd) \rightarrow d^*_{X^2-Y^2}(Pd)$ $d_{XZ1}(Pd) \rightarrow d^*_{X^2-Y^2}(Pd)$	89 10	0.71	1734	0.000
T_2 (T_{Pd_XZ})	$d_{XZ1}(Pd) \rightarrow d^*_{X^2-Y^2}(Pd)$ $d_{XZ2}(Pd) \rightarrow d^*_{X^2-Y^2}(Pd)$	38 37	1.11	1113	0.000
T_3 (T_{Pd_YZ})	$d_{YZ}(Pd) \rightarrow d^*_{X^2-Y^2}(Pd)$ π_{BL} (210) $\rightarrow d^*_{X^2-Y^2}(Pd)$ $d_{XZ2}(Pd) \rightarrow d^*_{X^2-Y^2}(Pd)$	58 14 10	1.27	974	0.000
T_4 (T_{CS_YZ})	$d_{YZ}(Ru) \rightarrow d^*_{X^2-Y^2}(Pd)$	99	1.69	734	0.000
T_5 (T_{Pd_XY})	$d_{XY2}(Pd) \rightarrow d^*_{X^2-Y^2}(Pd)$ $d_{XY1}(Pd) \rightarrow d^*_{X^2-Y^2}(Pd)$ σ_{BL} (211) $\rightarrow d^*_{X^2-Y^2}(Pd)$	62 21 11	1.74	711	0.000
T_6 (T_{CS_XZ})	$d_{XZ}(Ru) \rightarrow d^*_{X^2-Y^2}(Pd)$	98	1.85	671	0.000
T_7 (T_{CS_XY})	$d_{XY}(Ru) \rightarrow d^*_{X^2-Y^2}(Pd)$	99	1.85	670	0.000
T_8 (T_{BL1_YZ})	$d_{YZ}(Ru) \rightarrow \pi^*_{BL1}$ $d_{YZ}(Ru) \rightarrow \pi^*_{BL4}$	79 13	2.15	575	0.000
T_9 (T_{BL1_XZ})	$d_{XZ}(Ru) \rightarrow \pi^*_{BL1}$	84	2.29	541	0.000
T_{10} (T_{BL4_YZ})	$d_{YZ}(Ru) \rightarrow \pi^*_{BL4}$ $d_{XY}(Ru) \rightarrow \pi^*_{BL1}$ $d_{YZ}(Ru) \rightarrow \pi^*_{BL1}$	32 17 14	2.32	533	0.000
T_{11} (T_{BL1_XY})	$d_{XY}(Ru) \rightarrow \pi^*_{BL1}$ $d_{YZ}(Ru) \rightarrow \pi^*_{BL4}$	70 16	2.35	527	0.000

[a] Weights larger than 10%.

Table 5. Driving forces (ΔG), reorganization energies (λ_D and λ_A), potential couplings ($V_{D/A,max}$) and rate constants (k) for pairs of states.

donor → acceptor	ΔG (eV)	λ_i (eV)	$V_{D/A,max}$ (eV)	k_i (s^{-1})	$1/k_i$ (fs)
$T_{BL1\_XZ} \rightarrow T_{CS\_XZ}$	-0.692	0.463 0.453	0.027	5.89×10^{12} 5.25×10^{12}	170 190
$T_{BL1\_YZ} \rightarrow T_{CS\_YZ}$	-0.709	0.519 0.475	0.023	6.37×10^{12} 4.25×10^{12}	157 235

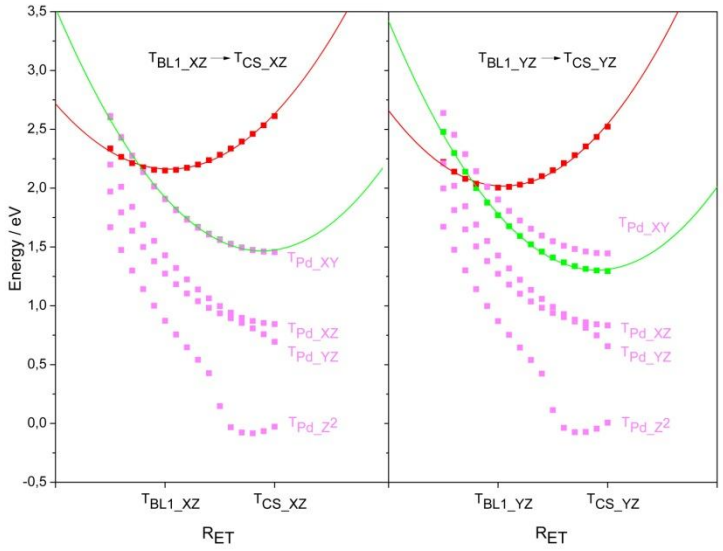

Figure 7. Calculated diabatic PECs of two pairs of donor (T_{BL1}, red squares) and acceptor (T_{CS}, green squares) states obtained at the TDDFT level of theory along a LICC (R_{ET}). A quadratic polynomial was fitted to the data sets. The energies of the four T_{Pd} states (pink squares) are indicated.

Analogous to section 3.2, the ET rates for the two pairs $T_{BL1\_XZ} \rightarrow T_{CS\_XZ}$ and $T_{BL1\_YZ} \rightarrow T_{CS\_YZ}$ are investigated by semi-classical Marcus theory (Figure 7 and Table 5). The obtained diabatic PECs exhibit a typical parabolic shape and the associated driving forces have negative values. It is also seen that for both pairs of states the crossing occurs in the inverted region (*i.e.* $\Delta G < -\lambda$). The calculated rates are comprised between 4.25×10^{12} and 6.37×10^{12} s^{-1}, which correspond to inverse rate constants of about 150-250 fs (Table 5). Hence, the $T_{BL1} \rightarrow T_{CS}$ ET rates of **RuPdCl$_1$** are about 10^5-10^6 times larger than for **RuPdCl$_2$**. This demonstrates that the dissociation of a chlorine ion produces a strong increase in the ET efficiency from the photosensitizer towards the catalytic center.

The $T_{BL1} \rightarrow T_{Pd}$ rates of **RuPdCl$_1$** were not calculated. However, the presence of T_{Pd} states in the low energy region of **RuPdCl$_1$** (Figure 7) suggests that a population transfer to these states can occur with similar rates as for **RuPdCl$_2$**. Because these rates have a comparable magnitude as the $T_{BL1} \rightarrow T_{CS}$ rates of **RuPdCl$_1$**, it appears that in **RuPdCl$_1$** the ET to the T_{CS} states competes

with the ET to the T_{Pd} states. Similarly to **$RuPdCl_2$** the population of the T_{Pd} or T_{CS} states of **$RuPdCl_1$** might lead to an additional dissociation or degradation of the catalytic center.

4. Discussions and conclusions

Quantum chemistry calculations in conjunction with the Marcus theory of ET were performed in order to shed light on the competitive relaxation pathways that can be reached following an excitation in the longer wavelength range of the **$RuPdCl_2$** absorption spectrum. The energies, orbital characters and geometries of the relevant triplet states were calculated using TDDFT, while PECs were constructed in order to determine the ET rates based on semi-classical Marcus theory. The theoretical results show that after the initial excitation, ISC leads most likely to the population of T_{BL1} states.

The direct ET process from the T_{BL1} states toward the catalytic center (*i.e.* T_{CS} states) has been evaluated and inverse rate constants comprised between 1400 ps and 134 ns have been obtained. The rather large values of these time constants indicate that this ET is a slow process for **$RuPdCl_2$**. Time-resolved measurements[9],[15] reported time constants of 310 ps (in acetonitrile), 740 ps (in dichloromethane) and larger than 800 ps (in gas phase), and were assigned to an ET from the tpphz ligand toward the catalytic center. The calculated time constant of 1400 ps for the $T_{BL1\_XY} \rightarrow T_{CS\_YZ}$ pair, which involves the highest T_{BL1} and lowest T_{CS} states, is in overall agreement with the experimental values. However, the generally larger time constants obtained for the other $T_{BL1} \rightarrow T_{CS}$ pairs indicate that these pairs are not associated with the measured ET process. Because higher excited states might also be populated in the experiment, it is likely that contributions of the higher T_{BL} states (*i.e.* T_{BL2}, T_{BL3} and T_{BL4}) are involved in the experimentally determined rates. Indeed, population of these T_{BL} states is energetically more favorable for an efficient ET to the T_{CS} states (*i.e.* associated with smaller time constants). Therefore, the obtained computational results indicate that an initial excitation in the longer wavelength part of the **$RuPdCl_2$** absorption spectrum is detrimental for the charge separation process.

The theoretical calculations revealed the presence of four low-energy T_{Pd} states, and their contribution to the **$RuPdCl_2$** photophysics was investigated for the first time. The calculated rates for the $T_{BL1} \rightarrow T_{Pd}$ transfer are about 10^4-10^7 times larger than the rates obtained for the $T_{BL1} \rightarrow T_{CS}$ transfer. Therefore, these results show that after population of the T_{BL1} states the transfer almost solely occurs toward the T_{Pd} states. Such a population transfer describes an electron recombination from the tpphz ligand to the ruthenium in conjunction with an energy transfer to the palladium. Therefore, the population of the T_{Pd} states annihilates the charge separation process by re-reducing the Ru atom, but transfers energy to the catalytic center. The further role of the T_{Pd} states can only be speculated, (i) due to their low energies they might lead to a relaxation process back to the **$RuPdCl_2$** ground state (S_0), which would correspond to a complete deactivation channel or, (ii) because they promote an electron to the anti-bonding orbital $d^*_{X^2-Y^2}$(Pd), they might facilitate an alteration of the catalytic center by *e.g.* inducing Cl^- dissociation. The latter possibility finds support in the previous literature. Indeed, in the initial paper[8] on **$RuPdCl_2$** it was proposed that after a chloride loss an ET to the Pd center occurs, whereas in a following work[9] it was assumed that the Cl^- dissociates quasi-instantaneously upon population of the T_{CS} state. Furthermore, it was experimentally proven[14] that during the catalysis, **$RuPdCl_2$** presents a decomposition of the catalytic center resulting in the formation of Pd colloids. Even if the exact mechanism of the Pd-Cl bond breaking still needs to be clarified, it is proposed here that the energy transfer occurring through the population of the T_{Pd} states is responsible for Cl^- dissociation. Additionally, the option (ii) is also supported by the fact that option (i) appears in contradiction with the increased catalytic efficiency of **$RuPdCl_2$** for longer excitation wavelengths[10], because option (i) only leads to a deactivation of the photocatalyst.

The effect of chloride loss was investigated by considering the **$RuPdCl_1$** system. The study of the excited states demonstrated that the absorption spectrum of **$RuPdCl_1$** is very similar to **$RuPdCl_2$** and that an excitation in the longer wavelength range, followed by ISC, populates T_{BL1} states. The calculated $T_{BL1} \rightarrow T_{CS}$ ET rates of **$RuPdCl_1$** are about 10^5-10^6 times larger than for

RuPdCl$_2$. This highlights that the dissociation of a chlorine ion strongly facilitates the generation of the charge separated state. Furthermore, from the presence of low-energy T_{Pd} states in **RuPdCl$_1$** it is inferred that the population transfer to these states competes with the charge separation process. Similarly to **RuPdCl$_2$**, it is proposed that population of T_{Pd} states will lead to an additional degradation of the catalytic center that might provide a mechanism for the formation of metal colloids.

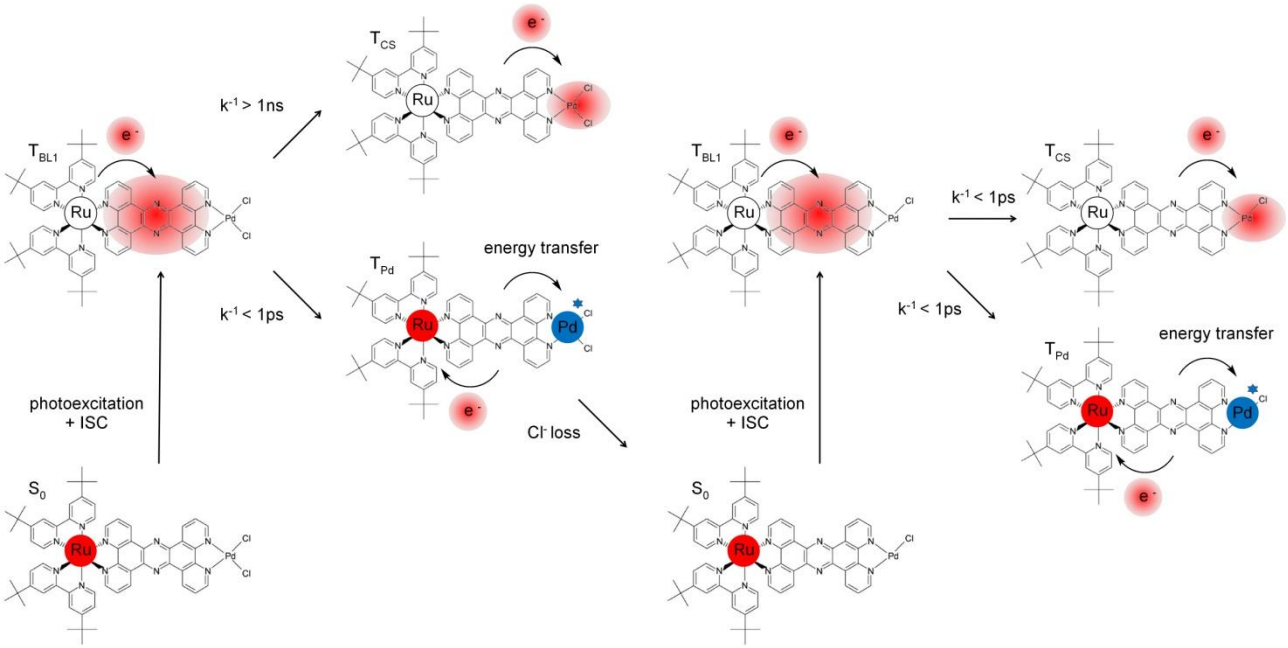

Figure 8. Schematic representation of the theoretically deduced photochemical mechanism.

In summary, the theoretical results presented in this work point to the following mechanism (Figure 8): (i) excitation in the longer wavelength part of the absorption spectrum (*i.e.* S_2 state), (ii) direct population of T_{BL1} states via ISC, (iii) fast population of T_{Pd} states (< 1 ps), (iv) dissociation of a Cl^- and formation of **RuPdCl$_1$**, (v) re-excitation and direct population of T_{BL1} states via ISC, (vi) competitive transfers (< 1 ps) to charge separated T_{CS} states (realizing a first electron transfer toward the catalytic center) and to T_{Pd} states (possibly leading to an additional alteration of the catalytic center). In this scheme, it is suggested that the alteration of the catalytic center is required to generate efficient charge separation and that this alteration provides one element explaining the

increased catalytic efficiency of **$RuPdCl_2$** for an excitation in the longer wavelength part of the absorption spectrum.

To validate the obtained mechanism, further studies should focus on the contribution of higher excited states as well as on the stable photocatalysts based on platinum instead of palladium. Additionally, the second electron transfer processes should be investigated in order to elucidate the mechanisms leading to catalytic activity and to the formation of molecular hydrogen.

Acknowledgments

This work is supported by the Narodowe Centrum Nauki (NCN) (project No. 2014/14/M/ST4/00083). S.K. thanks the Thuringian State Government for financial support within the ACP Explore project. The calculations have been performed at the Universitätsrechenzentrum of the Friedrich-Schiller University of Jena and at the Wrocław Centre for Networking and Supercomputing (grant No. 384). Furthermore, we are grateful for the support of the COST Action CM1202 Perspect-H2O.

Keywords

photocatalysis; density functional calculations; electron transfer; quantum chemistry; water splitting

Table of Contents

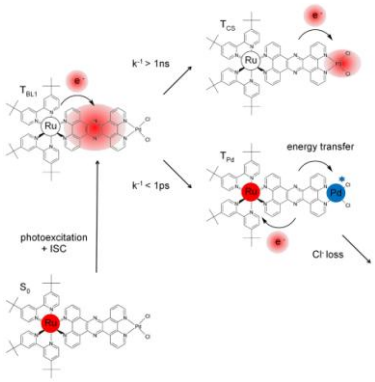

The way an electron moves in a molecular photocatalyst is investigated with quantum chemistry calculations. Photoexcitation transfers the electron to the bridging ligand. Then, it can choose between two pathways (i) moving to the catalytic center, or (ii) moving back to the ruthenium, while energy is transferred to the palladium. Channel (ii) is more favorable in the unaltered photocatalyst, but after Cl^- loss both channels become equally accessible.

References

[1] C. S. Ponseca, P. Chábera, J. Uhlig, P. Persson, V. Sundström, *Chem. Rev.* **2017**, *117*, 10940–11024.
[2] A. J. Nozik, J. Miller, *Chem. Rev.* **2010**, *110*, 6443–6445.
[3] D. G. Nocera, *Acc. Chem. Res.* **2012**, *45*, 767–776.
[4] D. G. Nocera, *Acc. Chem. Res.* **2017**, *50*, 616–619.
[5] V. Balzani, A. Juris, M. Venturi, S. Campagna, S. Serroni, *Chem. Rev.* **1996**, *96*, 759–833.
[6] E. S. Andreiadis, M. Chavarot-Kerlidou, M. Fontecave, V. Artero, *Photochem. Photobiol.* **2011**, *87*, 946–964.
[7] V. Artero, M. Chavarot-Kerlidou, M. Fontecave, *Angew. Chemie - Int. Ed.* **2011**, *50*, 7238–7266.
[8] S. Rau, B. Schäfer, D. Gleich, E. Anders, M. Rudolph, M. Friedrich, H. Görls, W. Henry, J. G. Vos, *Angew. Chem. Int. Ed.* **2006**, *45*, 6215–6218.
[9] S. Tschierlei, M. Presselt, C. Kuhnt, A. Yartsev, T. Pascher, V. Sundström, M. Karnahl, M. Schwalbe, B. Schäfer, S. Rau, et al., *Chem. Eur. J.* **2009**, *15*, 7678–7688.
[10] S. Tschierlei, M. Karnahl, M. Presselt, B. Dietzek, J. Guthmuller, L. González, M. Schmitt, S. Rau, J. Popp, *Angew. Chem. Int. Ed.* **2010**, *49*, 3981–3984.
[11] J. Guthmuller, L. González, *Phys. Chem. Chem. Phys.* **2010**, *12*, 14812–14821.
[12] L. Zedler, J. Guthmuller, I. Rabelo de Moraes, S. Kupfer, S. Krieck, M. Schmitt, J. Popp, S. Rau, B. Dietzek, *Chem. Commun.* **2014**, *50*, 5227–5229.
[13] M. Wächtler, J. Guthmuller, S. Kupfer, M. Maiuri, D. Brida, J. Popp, S. Rau, G. Cerullo, B. Dietzek, *Chem. - A Eur. J.* **2015**, *21*, 7668–7674.
[14] M. G. Pfeffer, B. Schäfer, G. Smolentsev, J. Uhlig, E. Nazarenko, J. Guthmuller, C. Kuhnt, M. Wächtler, B. Dietzek, V. Sundström, et al., *Angew. Chem. Int. Ed.* **2015**, *54*, 5044–5048.
[15] D. Imanbaew, J. Lang, M. F. Gelin, S. Kaufhold, M. G. Pfeffer, S. Rau, C. Riehn, *Angew. Chemie Int. Ed.* **2017**, *56*, 1–6.
[16] M. G. Pfeffer, T. Kowacs, M. Wächtler, J. Guthmuller, B. Dietzek, J. G. Vos, S. Rau, *Angew. Chem. Int. Ed.* **2015**, *54*, 6627–6631.
[17] M. Karnahl, C. Kuhnt, F. Ma, A. Yartsev, M. Schmitt, B. Dietzek, S. Rau, J. Popp, *ChemPhysChem* **2011**, *12*, 2101–2109.
[18] M. Karnahl, C. Kuhnt, F. W. Heinemann, M. Schmitt, S. Rau, J. Popp, B. Dietzek, *Chem. Phys.* **2012**, *393*, 65–73.
[19] M. G. Pfeffer, L. Zedler, S. Kupfer, M. Paul, M. Schwalbe, K. Peuntinger, D. M. Guldi, J. Guthmuller, J. Popp, S. Gräfe, et al., *Dalt. Trans.* **2014**, *43*, 11676–11686.
[20] R. A. Marcus, *J. Chem. Phys.* **1956**, *24*, 966–978.
[21] R. A. Marcus, *J. Chem. Phys.* **1965**, *43*, 679–701.
[22] A. Koch, D. Kinzel, F. Dröge, S. Gräfe, S. Kupfer, *J. Phys. Chem. C* **2017**, *121*, 16066–16078.
[23] M. J. Frisch, G. W. Trucks, H. B. Schlegel, G. E. Scuseria, M. A. Robb, J. R. Cheeseman, G. Scalmani, V. Barone, B. Mennucci, G. A. Petersson, et al., *Gaussian 09, Revision A.02*, Gaussian, Inc., Wallingford CT, **2009**.
[24] A. D. Becke, *J. Chem. Phys.* **1993**, *98*, 5648–5652.
[25] C. Lee, W. Yang, R. G. Parr, *Phys. Rev. B* **1988**, *37*, 785–789.
[26] D. Andrae, U. Häußermann, M. Dolg, H. Stoll, H. Preuß, *Theor. Chim. Acta* **1990**, *77*, 123–141.
[27] P. C. Hariharan, J. A. Pople, *Theor. Chim. Acta* **1973**, *28*, 213–222.
[28] S. Kupfer, M. Wächtler, J. Guthmuller, J. Popp, B. Dietzek, L. González, *J. Phys. Chem. C* **2012**, *116*, 19968–19977.
[29] C. Reichardt, M. Pinto, M. Wächtler, M. Stephenson, S. Kupfer, T. Sainuddin, J. Guthmuller, S. A. McFarland, B. Dietzek, *J. Phys. Chem. A* **2015**, *119*, 3986–3994.

[30] C. Latouche, D. Skouteris, F. Palazzetti, V. Barone, *J. Chem. Theory Comput.* **2015**, *11*, 3281–3289.
[31] J. Tomasi, B. Mennucci, R. Cammi, *Chem. Rev.* **2005**, *105*, 2999–3093.
[32] L. G. C. Rego, V. S. Batista, *J. Am. Chem. Soc.* **2003**, *125*, 7989–7997.
[33] R. Borrelli, M. Di Donato, A. Peluso, *J. Chem. Theo. Comput.* **2007**, *3*, 673–680.
[34] I. Kondov, M. Čížek, C. Benesch, H. Wang, M. Thoss, *J. Phys. Chem. C* **2007**, *111*, 11970–11981.
[35] J. Li, I. Kondov, H. Wang, M. Thoss, *J. Phys. Condens. Matter* **2015**, *27*, 134202.
[36] S. Kupfer, D. Kinzel, M. Siegmann, J. Philipp, B. Dietzek, S. Gräfe, *J. Phys. Chem. C* **2018**, *122*, 3273–3285.
[37] E. Sim, N. Makri, *J. Phys. Chem. B* **1997**, *101*, 5446–5458.
[38] M. Richter, B. P. Fingerhut, *J .Chem. Phys.* **2017**, *146*, 214101.
[39] L. Hu, M. Farrokhnia, J. Heimdal, S. Shleev, L. Rulíšek, U. Ryde, *J. Phys. Chem. B* **2011**, *115*, 13111–13126.
[40] J. Blumberger, *Phys. Chem. Chem. Phys.* **2008**, *10*, 5651–5667.
[41] H. Oberhofer, J. Blumberger, *J. Chem. Phys.* **2009**, *131*, 64101.
[42] A. R. Menzeleev, N. Ananth, T. F. Miller III, *J .Chem. Phys.* **2011**, *135*, 74106.
[43] L. W. Ungar, N. F. Scherer, G. A. Voth, *Biophys. J.* **1997**, *72*, 5–17.
[44] T. Kubař, M. Elstner, *J. Phys. Chem. B* **2008**, *112*, 8788–8798.
[45] C. A. Hurd, N. A. Besley, D. Robinson, *J. Comput. Chem.* **2017**, *38*, 1431–1437.
[46] M.-L. Tan, E. A. Dolan, T. Ichiye, *J. Phys. Chem. B* **2004**, *108*, 20435–20441.
[47] C. Daniel, *Coord. Chem. Rev.* **2015**, *282–283*, 19–32.
[48] M. Jäger, L. Freitag, L. González, *Coord. Chem. Rev.* **2015**, *304–305*, 146–165.
[49] A. D. Laurent, D. Jacquemin, *Int. J. Quantum Chem.* **2013**, *113*, 2019–2039.
[50] T. Yanai, D. P. Tew, N. C. Handy, *Chem. Phys. Lett.* **2004**, *393*, 51–57.
[51] M. J. G. Peach, D. J. Tozer, *J. Phys. Chem. A* **2012**, *116*, 9783–9789.
[52] H. Torieda, K. Nozaki, A. Yoshimura, T. Ohno, *J. Phys. Chem. A* **2004**, *108*, 4819–4829.
[53] D. M. Adams, L. Brus, C. E. D. Chidsey, S. Creager, C. Creutz, C. R. Kagan, P. V. Kamat, M. Lieberman, S. Lindsay, R. A. Marcus, et al., *J. Phys. Chem. B* **2003**, *107*, 6668–6697.
[54] R. Marcus, N. Sutin, *Biochim. Biophys. Acta-Reviews Bioenerg.* **1985**, *811*, 265–322.